LANGMUIR

pubs.acs.org/Langmuir Article

Complex Formation of Silica Nanoparticles with Collagen: Effects of the Conformation of Collagen

Ken Terao,* Mari Otsubo, and Masahiro Abe

Cite This: *Langmuir* 2020, 36, 14425−14431 Read Online

ACCESS | Metrics & More | Article Recommendations | Supporting Information

ABSTRACT: Negatively charged Ludox silica nanoparticles (SiNPs) form a complex with atelocollagen (AC) in acidic buffers (pH = 4 or 3). AC is a low-immunogenic derivative of collagen obtained by the removal of N- and C-terminal telopeptide components. Mixed solutions of negatively charged SiNPs and AC were turbid, while positively charged SiNPs (Ludox CL) did not form a complex with AC in pH 4 buffer, indicating that electrostatic attraction is the dominant force to form the complex. Small-angle X-ray scattering (SAXS) and circular dichroism (CD) measurements were made for AC and Ludox LS (or CL) solutions in acetate buffer (pH 4.0) and citrate buffer (pH 3.0). The CD data showed that the stability of the triple helical structure of AC in the buffers is not affected by the complexation. The resulting complex consisting of triple helical AC and SiNPs did not influence the SAXS profile except for the lowest q region investigated. On the contrary, different scattering profiles were observed for the single chain AC and SiNP mixture indicating densely packed SiNPs in the complex. This scattering behavior was fairly explained in terms of the sticky hard sphere model (SHSM). This AC conformation-dependent complexation may be because of the hydrogen bonding interaction between the single chain AC and SiNPs. The temperature-induced change of the complex formation can be applied for thermoresponsive hybrid materials.

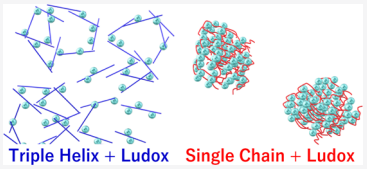

INTRODUCTION

Complex formation behavior of nanoparticles and proteins has attracted significant attention for potential application such as in drug delivery systems[1] and biosensors.[2] Thus, intermolecular interactions between silica nanoparticles (SiNP) and proteins and their complex formation were widely investigated in the past two decades.[3] Through light, small-angle X-ray, and small-angle neuron scattering techniques, the intermolecular interactions and structure of aggregates consisting of SiNPs and globular proteins have been studied[4−12] to elucidate that electrostatic attraction plays an important role. The structure factor of the densely packed SiNPs was clearly observed in the scattering vector range of the small-angle X-ray scattering (SAXS).[4,12]

Much work has been done for silica-collagen hybrid materials, owing to their use in biomedical applications.[13−17] These hybrid materials can be evaluated from the sol−gel reaction in the presence of collagen and/or gelatin in aqueous media.[18−21] The attractive interaction between silica and collagen plays an important role for the method; however, little work[22] has been done on the interaction. Collagen is the most abundant protein in mammals with a triple helical structure,[23,24] which unfolds in water at high temperatures. Considerably, the interactions between collagen model peptides and polyelectrolytes are influenced by the conformation of the peptides, that is, only triple helices can form a complex with the polyelectrolytes;[25−27] thus, the conformational change of proteins may cause a different complex structure. Therefore, we focused on the complex formation behavior of the SiNP and atelocollagen (AC) for which non-triple-helical telopeptides were removed by enzymatic reaction[28] to clarify how the triple helical structure causes the complex formation behavior with SiNPs. Thus, SAXS measurement of mixed solutions of SiNPs and AC was made at different temperatures below and above the melting temperature of the triple helices to investigate the relationship between collagen conformation and complexation. Circular dichroism (CD) measurement was made to verify whether the complex formation causes the stability of the triple helical structure of collagen.

EXPERIMENTAL SECTION

Samples. An AC sample (Koken, Japan), which is a highly purified type I collagen from the dermis of Australian bred calves, was used for this study. The molar mass of the triple helical AC is about 300 kg mol^{-1}. The solid sample was dried in a vacuum for 12 h prior to use. Suspensions of two SiNPs, Ludox LS and Ludox CL (Sigma-Aldrich), with a mass fraction of ca 30 wt % were diluted by a large amount of buffer. The obtained solutions were stable, and no precipitation was found at least one month. The latter SiNP (Ludox CL) was alumina coated. A certain amount of the suspension was weighed and lyophilized to estimate the actual concentration c_{NP} of the SiNP. Acetate buffer (40 mM, pH 4.0) and citrate buffer (40 mM, pH 3.0)

Received: September 30, 2020
Revised: November 3, 2020
Published: November 16, 2020

https://dx.doi.org/10.1021/acs.langmuir.0c02867
Langmuir 2020, 36, 14425−14431

were used as solvents because AC is not soluble at neutral pH. Solutions having mass concentrations, $2c_{AC}$ of AC and $2c_{NP}$ of SiNP, were prepared independently. Thereafter, the two solutions were mixed in equal volumes just before the measurement to obtain the solution with the concentrations of c_{AC} and c_{NP}. The pH value of the solution is substantially the same as that of the buffer because both c_{AC} and c_{NP} were at most 1.0 mg mL^{-1}.

Electrophoretic Light Scattering. Electrophoretic light scattering (ELS) measurement was made for Ludox LS, Ludox CL, and AC in the two buffers with an Otsuka zeta-potential analyzer at 25 °C. The solution mass concentrations (c_{AC} or c_{NP}) were set to be 1.0 mg mL^{-1}. The measurement was also made for the mixed solutions of Ludox CL and AC in the two buffers.

Circular Dichroism. CD measurement was made on a Jasco J720WO spectropolarimeter for AC with or without SiNPs in the buffers. Mass concentrations c_{AC} and c_{NP} were set to be 0.50 mg mL^{-1} and 0 or 0.50 mg mL^{-1}, respectively. CD spectra at 15 and 50 °C were recorded at the wavelength λ_0 in a vacuum ranging between 220 and 260 nm. It should be noted that substantially the same spectra were observed at least 30 min after the initial measurement. The ellipticity θ was recorded at λ_0 = 223 nm with raising the temperature from 15 to 50 °C at a rate of 0.5 °C min^{-1}.

Small-Angle X-Ray Scattering. SAXS measurement was made at the SPring-8 BL40B2 (Hyogo, Japan) for the SiNPs and the mixture of SiNP and AC in pH 3 and 4 buffers. Concentrations c_{AC} and c_{NP} were the same as that for the CD measurement (0.50 mg mL^{-1}). The camera length (the sample-to-detector distance) and λ_0 were set to be 4.2 m and 0.10 nm, respectively. A quartz capillary cell of 2.0 mmϕ was installed to the thermostatic cell holder controlled by a Peltier element. The intensity of the scattered light was integrated for 180 s with a Dectris Pilatus 3 2 M photon counting detector. The diffraction pattern of silver behenate was utilized to determine the magnitude q of the scattering vector at each pixel on the detector. A circular average procedure was employed by using SAngler software[29] to evaluate the scattering intensity $I(q)$ as a function of q. The scattering intensity was normalized by the intensity I_0 of the incident light detected at the lower end of the cell to compensate for both the intensity fluctuation of light source and solution transmittance. The excess scattering intensity $\Delta I(q)$ was evaluated as the difference of the normalized scattering intensity $I(q)/I_0$ between the solution and the solvent at each q. Because no concentration dependence of $\Delta I(q)/c_{NP}$ was observed for SiNP without AC, the structure factor $S(q)$ of the SiNP solution can be regarded as unity in the investigated q range. It is noted that no time dependence was observed for the current system at least 15 min. Some preliminary SAXS measurements were also made at the BL-6A beamline in KEK-PF (Ibaraki, Japan) to find the current experimental condition.

RESULTS AND DISCUSSION

ζ-potential. The obtained ζ-potential was positive for Ludox CL in the pH 4 buffer (+28 mV), while Ludox CL in the pH 3 buffer and Ludox LS at pH 3 and 4 have negative values, that is, −5, −5, and −8 mV, respectively. The negative ζ-potential of Ludox CL in the pH 3 buffer may be because of the desorption of aluminum ions.[30] The value for AC corresponds to +15 and +11 mV at pH 3 and 4, respectively, when assuming the equation for the spherical particle. Thus, AC and SiNPs except for Ludox CL at pH 4 are electrostatically attractive. Mixed solutions of Ludox CL and AC in the two buffers gave both positive values, +12 and +9 mV, respectively.

Turbidity of the Mixture. Photographs of the four mixed solutions with $c_{AC} = c_{NP}$ = 0.50 mg mL^{-1} are shown in Figure 1. The solutions were mixed in a glass vial placed on an aluminum block (∼10 °C) after being cooled in an ice bath (0 °C). As shown in Figure 1 (panel a), the left three solutions for which the ζ potentials of the SiNPs are negative are slightly

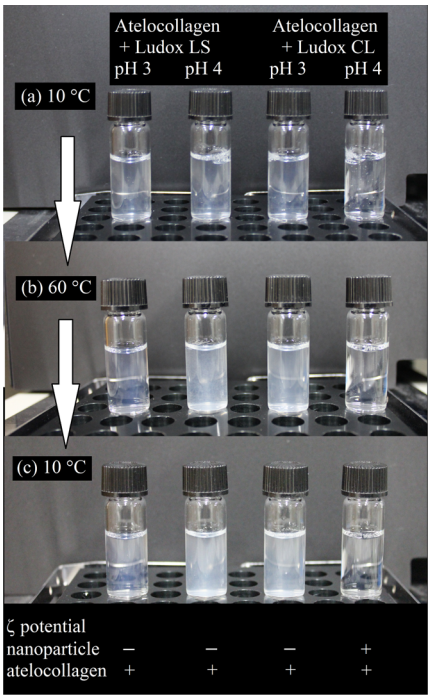

Figure 1. Photographs of mixed solutions of the AC and Ludox (LS or CL) in the indicated buffer at $c_{AC} = c_{NP}$ = 0.50 mg mL^{-1}. (a) 10 °C just after mixing, (b) 60 °C heated from 10 °C, and (c) 10 °C cooled from 60 °C.

turbid, whereas the other solution is almost transparent. Consequently, electrostatic attractive interactions are necessary to form a complex of SiNP and AC. The three left solutions became turbid more significantly (panel b) after heated to 60 °C in a water bath. The turbidity of the solution did not change even after cooling to 10 °C (panel c), indicating that the complexation behavior is not temperature-reversible. Precipitates were observed for the mixtures except for the right end solution. Moreover, fiber-like precipitates were found by visual observation for the left end solution (Ludox LS + AC at pH 3). This indicates that it is difficult to make light scattering measurement to obtain reproducible scattering data for the current systems.

Melting Behavior of the Triple Helical Structure of the AC. Figure 2 illustrates the wavelength dependence of the specific ellipticity $[\theta']$ for the AC with or without SiNP. A positive peak at about λ_0 = 223 nm is typical for the triple helical structure of the AC.[31] Panels (a) and (b) show the CD spectra of the mixed solutions prepared at 0 °C and measured at 15 °C, respectively. Substantially the same spectra for all the samples indicate that the local helical structure of the AC is free from the presence of SiNP, whereas a slightly smaller peak height for the mixed solution is most likely because of the large aggregates or the partially unfolded AC. In contrast, the $[\theta']$ values at 50 °C and those cooled to 15 °C are small and negative in the range of λ_0 < 240 nm, as illustrated in panels (c–f), indicating that AC behaves as single random coils in the solvents: The slight temperature dependence may not be owing to the formation of the triple helical structure taking into consideration that CD spectra of single chain collagen model peptides have slight temperature dependence.[32] Interestingly, all the CD spectra for the mixed solutions are substantially the same as those for AC without SiNPs. These results indicate that local conformation of the AC detected by

https://dx.doi.org/10.1021/acs.langmuir.0c02867
Langmuir 2020, 36, 14425−14431

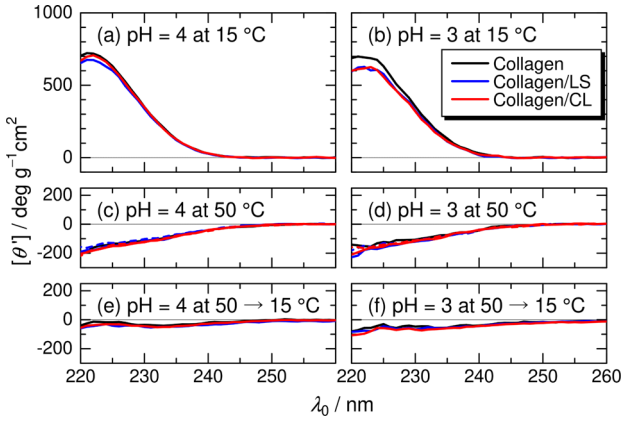

Figure 2. CD spectra for the AC (black), mixed solution of the AC and Ludox LS (blue), or Ludox CL (red) at c_{AC} = 0.50 mg mL^{-1}. (a) pH = 4 at 15 °C, (b) pH = 3 at 15 °C, (c) pH = 4 at 50 °C, and (d) pH = 3 at 50 °C. Solid and dashed curves in panels (c,d) are for the solutions prepared at 50 °C and 0 °C, respectively. (e,f) show the data measured at 15 °C cooled from 50 °C at pH = 4 and 3, respectively.

the CD measurement is not significantly affected by the SiNPs even though they form a complex in the buffers.

The CD intensity of AC with and without the SiNP was measured at λ_0 = 223 nm to estimate the melting temperatures of the triple helical structure with raising the temperature at the rate of 0.5 °C min^{-1}. The values of $[\theta']$ are mostly independent of T below 30 °C and decrease rapidly between 35 and 40 °C, as illustrated in Figure 3. The melting

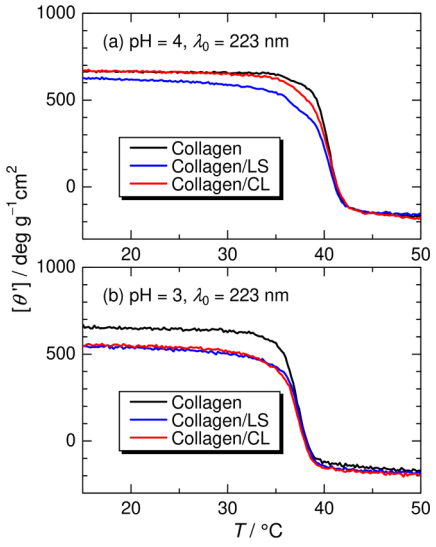

Figure 3. Temperature dependence of $[\theta']$ for the indicated AC and the mixed solutions at pH = 4 (a) and pH = 3 (b). The signal was acquired at λ_0 = 223 nm. The temperature raising rate was 0.5 °C min^{-1}.

temperature of the AC is free from the existence of the SiNP. This indicates that the SiNPs do not significantly affect the stability of the triple helical structure of the AC. Smaller $[\theta']$ values for the mixed solutions at low temperatures are most likely due to the large aggregates or partially unfolded conformation as in the case of the CD spectra in Figure 2.

Scattering Behavior of Silica Particles with and without AC. Figure 4 illustrates SAXS data for Ludox LS and CL in the two buffers. As shown in panel (a), the data for

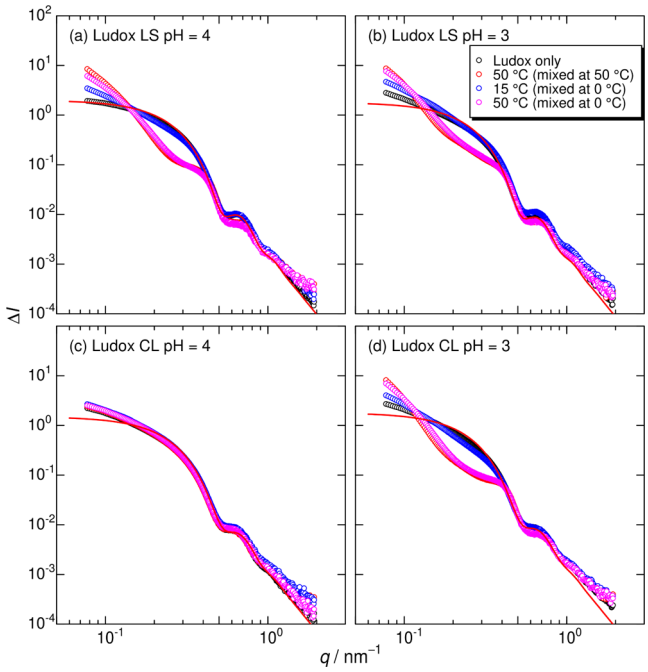

Figure 4. Double logarithmic plots for the excess scattering intensity ΔI vs q for Ludox LS in the pH 4 buffer (a), Ludox LS in the pH 3 buffer (b), Ludox CL in the pH 4 buffer (c), and Ludox CL in the pH 3 buffer (d) with or without the AC at c_{NP} = 0.50 mg mL^{-1} at indicated temperatures. Solid red curves indicate the calculated values for polydisperse spheres (see text).

the Ludox LS solution (black circles) at pH 4 without AC are typical for the sphere with a certain size distribution. Moreover, if it is modeled by the sphere for which the size distribution is assumed by a log−normal distribution, the z-average particle scattering function $P_z(q)$ (or the form factor) can be expressed as

$$P_z(q) = \frac{\int_0^\infty \Phi^2(\sqrt[3]{3V/4\pi}\,q)Vw(V)\mathrm{d}V}{\int_0^\infty Vw(V)\mathrm{d}V} \quad (1)$$

$$\Phi(x) = \frac{3(\sin x - x\cos x)}{x^3} \quad (2)$$

$$w(V) = \frac{1}{\sqrt{2\pi}\sigma_V V}\exp\left\{-\frac{[\ln(V/V_m)]^2}{2\sigma_V{}^2}\right\} \quad (3)$$

where V_m and σ_V are the parameters of volume dispersion. The median volume V_m is related to the median radius R_m, where $V_m = 4\pi R_m{}^3/3$. The calculated red curve quantitatively describes the experimental data for Ludox LS in the pH 4 buffer when we choose R_m = 8.6 nm and σ_V = 0.40. The σ_V value corresponds to the dispersity index Đ of 1.17, which is defined as the ratio of weight- to number-average molar masses. The slight upward deviation behavior at the high q region is most likely because of the roughness of the sphere surface and/or the internal structure of SiNPs. On the contrary, a higher scattering intensity was found in the lowest q region investigated at pH 3, as illustrated in Figure 4b, suggesting slight aggregation. The data for Ludox LS at pH 3 can be reproduced using the same parameters except for the lowest q region. Likewise, the scattering profiles for the Ludox CL in the two buffers [Figure 4 c,d] are explained by the

https://dx.doi.org/10.1021/acs.langmuir.0c02867
Langmuir 2020, 36, 14425−14431

polydisperse sphere with R_m = 8.6 nm and σ_V = 0.45 (Đ = 1.22) except for the low q end. This result also suggests slight aggregation in the solvents.

Figure 4c shows the data for the transparent mixture in which the ζ potentials of both the two components are positive. It is evident that the AC does not cause any significant difference in the SAXS profile, indicating that no interactions between the two species and the scattering intensity from the AC is small enough to be ignored except for the high q region (q > 1 nm^{-1}). This is reasonable because the calculated scattering intensities of AC taking the SAXS contrast factor[33] into account are much smaller than SiNP in the range of q < 0.8 nm^{-1}, as shown in Figure S1 in Supporting Information. Indeed, the actual scattering intensity from AC in the buffers was less than 1/100 at q = 0.1 nm^{-1} and 1/10 at 1 nm^{-1} compared with SiNPs.

In contrast, the scattering profiles for the other mixed solution systems are appreciably different from the SiNP without the AC, suggesting an aggregation consisting of the SiNP and AC. This result is consistent with the visual observation in Figure 1. The ΔI data for the mixed solution of the SiNP and AC at 15 °C except for that in Figure 4c are higher compared to that without the AC only below q = 0.2 nm^{-1}. Contrarily, much lower $\Delta I(q)$ at approximately q = 0.3 nm^{-1} for the mixed solution at 50 °C indicates interparticle interference effects for the densely aggregated SiNP particles. This significant difference at the two temperatures suggests that most SiNPs form a complex with the AC at 50 °C. The data for the solution heated from 15 to 50 °C is almost the same as that at 50 °C mixed at the same temperature. They can thus be regarded as the equilibrium states. Furthermore, the scattering data cooled from 50 to 15 °C is almost the same as that at 50 °C (Figure S2). This shows that the aggregating structure is determined by the conformation of AC. In summary, complex formation is mainly caused by the electrostatic attractive force, but the resulting aggregation structure strongly depends on the conformation of the AC, that is, a triple helix or single random coil. Schematically, the difference in the aggregation structures is illustrated in Figure 5.

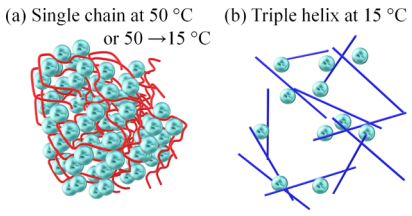

Figure 5. Schematic representation of complex formation of (a) triple helical AC (blue lines) with SiNP (spheres) at 15 °C and (b) single coil AC (red curves) with SiNP (spheres) at 50 °C or at 15 °C cooled from 50 °C.

Theoretical Analysis of the Structure Factor. Assuming size distribution of SiNPs are negligible, ΔI can be written as $\Delta I(q) \propto S(q)P(q)$ with $S(q)$ being the structure factor. Therefore, if we consider the scattering intensity from AC is negligible, $S(q)$ of SiNPs can be experimentally estimated by $S(q) = \Delta I_{mix}(q)/\Delta I_{SiNP}(q)$ where $\Delta I_{mix}(q)$ and $\Delta I_{SiNP}(q)$ denote the excess scattering intensities of mixed solution and SiNP solution, respectively. Figure 6 illustrates the obtained $S(q)$ for Ludox LS with AC at pH 4. While $S(q)$ for SiNP with

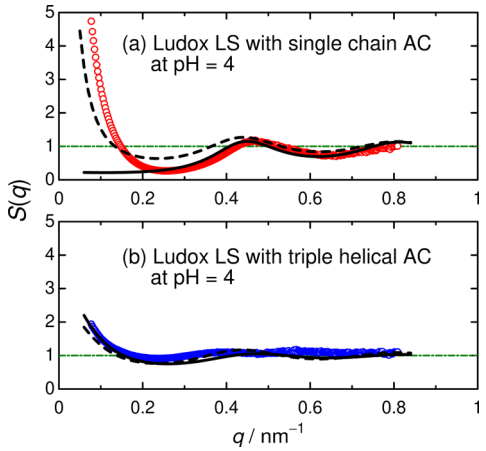

Figure 6. Plots of $S(q)$ vs q for (a) Ludox LS with single chain AC at 50 °C mixed at the same temperature and (b) Ludox LS with triple helical AC at 15 °C prepared at 0 °C both at pH = 4. Solid and broken curves are theoretical values for cases 1 and 2, respectively, with the parameters listed in Table 1. Dot-dashed lines, $S(q)$ = 1.

the triple-helical AC (panel b) is almost unity except for the low q region, significant q dependence is found for the mixture with single-chain AC (panel a). If it is expressed by the sticky hard sphere model (SHSM),[34] for which stickiness is introduced by the square-well potential with the well width Δ and depth u_0, $S(q)$ is expressed as[35,36]

$$S(q) = f(q, \phi_{NP}, \sigma_s, \Delta, u_0/k_BT) \quad (4)$$

where ϕ_{NP}, σ_s, k_B, and T are the volume fraction of nanoparticles, the diameter of the particles (= $2R_m$), the Boltzmann constant, and the absolute temperature, respectively. In the model, the pair potential is defined as the function of the distance r between two SiNPs to be $+\infty$, u_0, and 0 for $0 < r < \sigma_s$, $\sigma_s < r < \sigma_s + \Delta$, and $\sigma_s + \Delta < r$, respectively.

A curve fitting procedure was examined for the data in Figure 6a. Very small Δ value was estimated to be 0.15 nm ± 0.05 nm to reproduce the peak at q = 0.45 nm^{-1} because the peak position tends to decrease with increasing Δ, and indeed, the peak position is substantially free from the error range of Δ. When we choose Δ = 0.15 nm, ϕ_{NP} = 0.32, and $-u_0/k_BT$ = 3.6 (case 1), the obtained theoretical solid curve represents the experimental data in the range of q > 0.2 nm^{-1}. Much larger ϕ_{NP} than that in the actual solution (~0.00044, estimated from the SiNP density of 2.25 g mL^{-1})[5] indicates the densely packed SiNPs in the complex. The stickiness parameter τ^{-1} which is a measure of the stickiness and defined by $\tau^{-1} \equiv 12\Delta/(\sigma_s + \Delta) \exp(-u_0/k_BT)$ was calculated to be 3.8, which is the same order as the previously investigated value for SiNP and lysozyme.[5] The obtained values are, however, smaller than the critical value of 8.8,[5,37] indicating one phase region (no phase separation). Furthermore, the abruptly increasing behavior at a low q region with decreasing q cannot be explained with the parameters. Taking into consideration that the contour length (300 nm) of the AC chain is much longer than the diameter of SiNP (17 nm), the densely packed silica particles may be stabilized not only by the short-range attractive interactions characterized by u_0 and Δ but also by the middle range interaction through long AC chains. On the other hand, if we attempted to reproduce the whole range of the data (case 2), Δ = 0.15 nm, ϕ_{NP} = 0.12, and $-u_0/k_BT$ = 4.4 can be estimated.

https://dx.doi.org/10.1021/acs.langmuir.0c02867
Langmuir 2020, 36, 14425−14431

Table 1. Model Parameters for SiNPs with AC

SiNP	AC	pH	case	$-u_0/k_BT$	Δ/nm	ϕ_{NP}
Ludox LS	single chain	4	1	3.6 ± 0.4	0.15 ± 0.05	0.32
			2	4.4 ± 0.6	0.15 ± 0.05	0.12 ± 0.03
Ludox LS	triple helix	4	1	1.3	0.15[a]	0.32[a]
			2	3.9	0.15[a]	0.12[a]
Ludox LS	single chain	3	1	3.0 ± 0.4	0.15 ± 0.05	0.31
Ludox CL	single chain	3	1	3.6 ± 0.4	0.15 ± 0.05	0.32

[a]Assumed.

The obtained dashed curve cannot however reproduce the very low $S(q)$ value between q = 0.2 and 0.3 nm^{-1}. Because the SHSM only considers the short-range interaction, the case 1 is more favorable to reflect the characteristics of the local aggregation structure of the current system. The parameters are summarized in Table 1. The error range indicates that substantially the same theoretical curve can be obtained. The well width Δ is significantly smaller than that for the previously investigated silica-lysozyme system (1.2−1.7 nm).[5] This is consistent with that the single chain AC is much thinner than the diameter of lysozyme. It is however noticed that only the relative magnitude of each parameter may be meaningful because the absorbed AC chain on the SiNPs plays an important role for the attractive interaction between SiNPs, that is, the actual potential of each SiNP might be distorted from the spherical symmetry.

On the contrary, the parameters cannot be determined for Ludox LS with the triple helical AC (Figure 6b) because of the almost flat $S(q)$. If we assume Δ = 0.15 nm and ϕ_{NP} = 0.33, the theoretical solid curve calculated with $-u_0/k_BT$ = 1.3 can explain the experimental data. Similar theoretical values (dashed curve) can be evaluated with Δ = 0.15 nm, ϕ_{NP} = 0.12, and $-u_0/k_BT$ = 3.9; the $-u_0/k_BT$ values are much smaller than those for SiNP and single chain AC with the corresponding ϕ_{NP}. This result indicates that attractive interactions between SiNPs through the triple helical AC molecules are much weaker than that through the single chain AC.

Similar analysis was also examined for the mixed solution of the SiNPs and single chain AC at pH 3. Ignoring slight aggregation of SiNP in the buffer, $S(q)$ can be evaluated by the same method as that at pH 4. It should be noted that we omitted the $S(q)$ data for q < 0.13 nm^{-1} because appreciably larger $\Delta I(q)$ was observed than that for the theoretical value for the polydisperse sphere as shown in Figure 4. The resulting plot of $S(q)$ versus q is shown in Figure 7a. Ludox LS at pH = 3 has a weaker depression at q = 0.2−0.3 nm^{-1} than those at pH = 4, suggesting looser aggregates. Indeed, a theoretical analysis as the same method of the case 1 gives smaller $-u_0/k_BT$ with slightly smaller ϕ_{NP}. The stickiness τ^{-1} at pH 3 is therefore calculated to be a smaller value of 2.1 than 3.8 at pH 4. This pH dependence is most likely because of the smaller magnitude of the ζ potential at pH 3, in other words, weaker electrostatic attraction. On the other hand, $S(q)$ for the Ludox CL with the single chain AC at pH 3 shown in Figure 7b is close to that for the Ludox LS system at pH 4, suggesting different surface condition between Ludox LS and CL. The current analysis in terms of the SHSM supports the densely packed SiNPs in the complex consisting of SiNPs and single chain AC.

Origin of the Densely Packed SiNPs in the Complex. The above-mentioned analysis for the SAXS data clearly showed that only the single chain AC form a densely packed complex with negatively charged SiNPs even though the stability of a triple helical structure of AC is almost independent of the presence of SiNPs. The triple helical structure of collagen is stabilized by the hydrogen bonding, and hence, single chain collagen molecules have many free hydrogen-bonding sites. Therefore, the current result is most likely because the hydrogen-bonding interactions between the single chain AC and SiNPs are much more significant compared to that between triple helical AC and SiNP, even while the electrostatic attractive interactions are mandatory for the complexation. This finding may be applicable for the novel thermo-responsible nanoparticle-collagen hybrid materials.

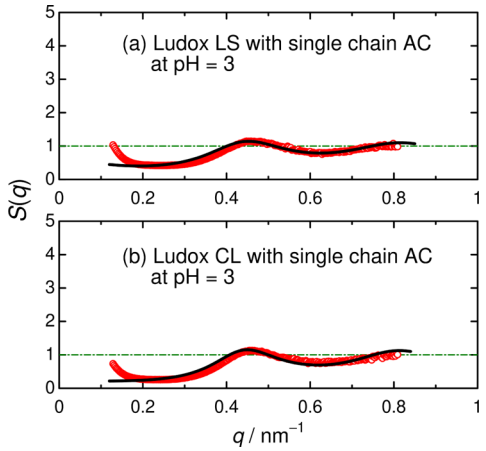

Figure 7. Plots of $S(q)$ vs q for (a) Ludox LS with single chain AC at 50 °C and (b) Ludox CL with single chain AC at 50 °C both at pH = 3. Solid curves are the theoretical curves for the SHSM theory with the parameters listed in Table 1. Dot-dashed lines, $S(q)$ = 1.

CONCLUSIONS

Positively charged AC and negatively charged SiNPs form a complex in the pH 3 and 4 buffers. Electrostatic attractive force is dominant to form the complex. The melting temperature of the triple helical structure is independent of the complex formation. The density of the SiNPs in the complex is not high when the AC retains the triple helical structure. In contrast, significantly dense SiNPs are obtained from the complex consisting of SiNP and the single chain AC, suggesting that not only electrostatic interactions but also hydrogen bonding interactions play important roles in the formation of the complex consisting of SiNPs and collagen.

ASSOCIATED CONTENT

Supporting Information

The Supporting Information is available free of charge at https://pubs.acs.org/doi/10.1021/acs.langmuir.0c02867.

https://dx.doi.org/10.1021/acs.langmuir.0c02867
Langmuir 2020, 36, 14425−14431

Estimation of the scattering intensity of SiNPs and AC and additional SAXS data (PDF)

AUTHOR INFORMATION

Corresponding Author

Ken Terao − *Department of Macromolecular Science, Graduate School of Science, Osaka University, Toyonaka, Osaka 560-0043, Japan;* orcid.org/0000-0001-7363-4491; Phone: +81 6 6850 5459; Email: kterao@chem.sci.osaka-u.ac.jp; Fax: +81 6 6850 5461

Authors

Mari Otsubo − *Department of Macromolecular Science, Graduate School of Science, Osaka University, Toyonaka, Osaka 560-0043, Japan*

Masahiro Abe − *Department of Macromolecular Science, Graduate School of Science, Osaka University, Toyonaka, Osaka 560-0043, Japan*

Complete contact information is available at: https://pubs.acs.org/10.1021/acs.langmuir.0c02867

Notes

The authors declare no competing financial interest.

ACKNOWLEDGMENTS

The authors are grateful to Prof. Takahiro Sato (Osaka Univ.) for fruitful discussion, to Prof. Emer. Kenji Okuyama (Tokyo Univ. Agric. and Tech) for collagen sample supply, to Mr. Koreyoshi Ogata (Osaka Univ.) for preliminary experiments, to Drs. Noboru Ohta (SPring-8), Nobutaka Shimizu. (KEK), and Noriyuki Igarashi (KEK) for SAXS measurement, and to the reviewers of the previous submission for the critical comments. The synchrotron radiation experiments were performed at the BL40B2 in SPring-8 with the approval of the Japan Synchrotron Radiation Research Institute (JASRI) (Proposal Nos. 2016A1053, 2016B1088, and 2019A1072) and at the BL-6A beamline in KEK-PF (2018G519). This work was partly supported by JSPS KAKENHI Grant Numbers JP17K05884, JP18H02020, and JP20H02788.

REFERENCES

(1) Jiang, W.; Kim, B. Y. S.; Rutka, J. T.; Chan, W. C. W. Nanoparticle-mediated cellular response is size-dependent. *Nat. Nanotechnol.* **2008**, *3*, 145−150.

(2) Phillips, R. L.; Miranda, O. R.; You, C.-C.; Rotello, V. M.; Bunz, U. H. F. Rapid and efficient identification of bacteria using gold-nanoparticle-poly(para-phenyleneethynylene) constructs. *Angew. Chem., Int. Ed.* **2008**, *47*, 2590−2594.

(3) Kumar, S.; Yadav, I.; Aswal, V. K.; Kohlbrecher, J. Structure and Interaction of Nanoparticle-Protein Complexes. *Langmuir* **2018**, *34*, 5679−5695.

(4) Bharti, B.; Meissner, J.; Findenegg, G. H. Aggregation of silica nanoparticles directed by adsorption of lysozyme. *Langmuir* **2011**, *27*, 9823−9833.

(5) Bharti, B.; Meissner, J.; Klapp, S. H. L.; Findenegg, G. H. Bridging interactions of proteins with silica nanoparticles: the influence of pH, ionic strength and protein concentration. *Soft Matter* **2014**, *10*, 718−728.

(6) Wang, J.; Jensen, U. B.; Jensen, G. V.; Shipovskov, S.; Balakrishnan, V. S.; Otzen, D.; Pedersen, J. S.; Besenbacher, F.; Sutherland, D. S. Soft interactions at nanoparticles alter protein function and conformation in a size dependent manner. *Nano Lett.* **2011**, *11*, 4985−4991.

(7) Yadav, I.; Kumar, S.; Aswal, V. K.; Kohlbrecher, J. Small-angle neutron scattering study of differences in phase behavior of silica nanoparticles in the presence of lysozyme and bovine serum albumin proteins. *Phys. Rev. E: Stat., Nonlinear, Soft Matter Phys.* **2014**, *89*, 032304.

(8) Yadav, I.; Aswal, V. K.; Kohlbrecher, J. Size-dependent interaction of silica nanoparticles with lysozyme and bovine serum albumin proteins. *Phys. Rev. E* **2016**, *93*, 052601.

(9) Yadav, I.; Kumar, S.; Aswal, V. K.; Kohlbrecher, J. Structure and Interaction in the pH-Dependent Phase Behavior of Nanoparticle-Protein Systems. *Langmuir* **2017**, *33*, 1227−1238.

(10) Kundu, S.; Das, K.; Mehan, S.; Aswal, V. K.; Kohlbrecher, J. Structure and interaction among protein and nanoparticle mixture in solution: Effect of temperature. *Chem. Phys. Lett.* **2015**, *641*, 68−73.

(11) Marichal, L.; Giraudon−Colas, G.; Cousin, F.; Thill, A.; Labarre, J.; Boulard, Y.; Aude, J.-C.; Pin, S.; Renault, J. P. Protein-Nanoparticle Interactions: What Are the Protein-Corona Thickness and Organization? *Langmuir* **2019**, *35*, 10831−10837.

(12) Stawski, T. M.; van den Heuvel, D. B.; Besselink, R.; Tobler, D. J.; Benning, L. G. Mechanism of silica-lysozyme composite formation unravelled by in situ fast SAXS. *Beilstein J. Nanotechnol.* **2019**, *10*, 182−197.

(13) Ono, Y.; Kanekiyo, Y.; Inoue, K.; Hojo, J.; Nango, M.; Shinkai, S. Preparation of Novel Hollow Fiber Silica Using Collagen Fibers as a Template. *Chem. Lett.* **1999**, *28*, 475−476.

(14) Heinemann, S.; Coradin, T.; Desimone, M. F. Bio-inspired silica-collagen materials: applications and perspectives in the medical field. *Biomater. Sci.* **2013**, *1*, 688−702.

(15) Chen, S.; Chinnathambi, S.; Shi, X.; Osaka, A.; Zhu, Y.; Hanagata, N. Fabrication of novel collagen-silica hybrid membranes with tailored biodegradation and strong cell contact guidance ability. *J. Mater. Chem.* **2012**, *22*, 21885−21892.

(16) Lee, E.-J.; Jun, S.-H.; Kim, H.-E.; Koh, Y.-H. Collagen-silica xerogel nanohybrid membrane for guided bone regeneration. *J. Biomed. Mater. Res., Part A* **2012**, *100*, 841−847.

(17) Lei, B.; Shin, K.-H.; Noh, D.-Y.; Jo, I.-H.; Koh, Y.-H.; Choi, W.-Y.; Kim, H.-E. Nanofibrous gelatin−silica hybrid scaffolds mimicking the native extracellular matrix (ECM) using thermally induced phase separation. *J. Mater. Chem.* **2012**, *22*, 14133.

(18) Coradin, T.; Bah, S.; Livage, J. Gelatine/silicate interactions: from nanoparticles to composite gels. *Colloids Surf. B Biointerfaces* **2004**, *35*, 53−58.

(19) Smitha, S.; Shajesh, P.; Mukundan, P.; Nair, T. D. R.; Warrier, K. G. K. Synthesis of biocompatible hydrophobic silica-gelatin nano-hybrid by sol-gel process. *Colloids Surf. B Biointerfaces* **2007**, *55*, 38−43.

(20) Setyawan, H.; Balgis, R. Mesoporous silicas prepared from sodium silicate using gelatin templating. *Asia-Pac. J. Chem. Eng.* **2012**, *7*, 448−454.

(21) Nojima, T.; Suzuki, S.; Iyoda, T. Atelocollagen-templated fabrication of tangled fibrous silica. *J. Mater. Chem. B* **2016**, *4*, 6640−6643.

(22) Bergman, I.; Nelson, E. S. The polymerization of silicic acid and its subsequent interaction with proteins and other hydrogen-bonding agents. *J. Colloid Sci.* **1962**, *17*, 823−837.

(23) Ramachandran, G. N.; Kartha, G. Structure of collagen. *Nature* **1954**, *174*, 269−270.

(24) Okuyama, K. Revisiting the molecular structure of collagen. *Connect. Tissue Res.* **2008**, *49*, 299−310.

(25) Terao, K.; Kanenaga, R.; Sato, T.; Mizuno, K.; Bächinger, H. P. Complex formation of collagen model peptides with polyelectrolytes and stabilization of the triple helical structure. *Macromolecules* **2012**, *45*, 392−400.

(26) Terao, K.; Kanenaga, R.; Yoshida, T.; Mizuno, K.; Bächinger, H. P. Temperature induced complex formation-deformation behavior of collagen model peptides and polyelectrolytes in aqueous solution. *Polymer* **2015**, *64*, 8−13.

(27) Ishida, S.; Yoshida, T.; Terao, K. Complex formation of a triple-helical peptide with sodium heparin. *Polym. J.* **2019**, *51*, 1181−1187.

(28) Stenzel, K. H.; Miyata, T.; Rubin, A. L. Collagen as a biomaterial. *Annu. Rev. Biophys. Bioeng.* **1974**, *3*, 231−253.
(29) Shimizu, N.; Yatabe, K.; Nagatani, Y.; Saijyo, S.; Kosuge, T.; Igarashi, N., Software development for analysis of small-angle X-ray scattering data. *AIP Conference Proceedings* 2016, *1741*, 050017.
(30) Van der Meeren, P.; Saveyn, H.; Bogale Kassa, S.; Doyen, W.; Leysen, R. Colloid−membrane interaction effects on flux decline during cross-flow ultrafiltration of colloidal silica on semi-ceramic membranes. *Phys. Chem. Chem. Phys.* **2004**, *6*, 1408−1412.
(31) Holmes, R.; Kirk, S.; Tronci, G.; Yang, X.; Wood, D. Influence of telopeptides on the structural and physical properties of polymeric and monomeric acid-soluble type I collagen. *Mater. Sci. Eng., C* **2017**, *77*, 823−827.
(32) Terao, K.; Mizuno, K.; Murashima, M.; Kita, Y.; Hongo, C.; Okuyama, K.; Norisuye, T.; Bächinger, H. P. Chain dimensions and hydration behavior of collagen model peptides in aqueous solution: [Glycyl-4(R)-hydroxyprolyl-4(R)-hydroxyproline](n), [glycylprolyl-4(R)-hydroxyproline](n), and some related model peptides. *Macromolecules* **2008**, *41*, 7203−7210.
(33) Glatter, O.; Kratky, O. *Small Angle X-ray Scattering*; Academic Press: London, 1982.
(34) Baxter, R. J. Percus-Yevick Equation for Hard Spheres with Surface Adhesion. *J. Chem. Phys.* **1968**, *49*, 2770−2774.
(35) Menon, S. V. G.; Manohar, C.; Rao, K. S. A New Interpretation of the Sticky Hard-Sphere Model. *J. Chem. Phys.* **1991**, *95*, 9186−9190.
(36) Hashimoto, T. *Principles and Applications of X-ray, Light and Neutron Scattering*; Kodansha: Tokyo, Japan, 2017.
(37) Miller, M. A.; Frenkel, D. Competition of percolation and phase separation in a fluid of adhesive hard spheres. *Phys. Rev. Lett.* **2003**, *90*, 135702.

https://dx.doi.org/10.1021/acs.langmuir.0c02867
Langmuir 2020, 36, 14425−14431